Observation of Hidden Fermi Surface Nesting in a Two Dimensional Conductor

Klaus Breuer,* Cristian Stagerescu,† and Kevin E. Smith‡
Department of Physics, Boston University, Boston, Massachusetts 02215

Martha Greenblatt and Kandalam Ramanujachary
Department of Chemistry, Rutgers University, Piscataway, New Jersey 08855
(Received 25 January 1996)

We report the first direct measurement of hidden Fermi surface nesting in a two dimensional conductor. The system studied was $Na_{0.9}Mo_6O_{17}$, and the measured Fermi surface consists of electron and hole pockets that can be combined to form sets of pseudo-one-dimensional Fermi surfaces, exhibiting the nesting necessary to drive a Peierls transition to a charge density wave state. The observed nesting vector is shown to be in excellent agreement with theory. [S0031-9007(96)00001-4]

PACS numbers: 71.18.+y, 73.20.Dx, 79.60.Bm

The concept of hidden Fermi surface nesting was developed to explain the existence of charge density waves (CDW) periodic lattice distortions (PLD) and Peierls transitions in both organic and inorganic *quasi-two-dimensional* (2D) conductors [1,2]. These phenomena are generally associated with *quasi-one-dimensional* (1D) solids, and originate from the existence of nested 1D Fermi surfaces. The transition to a CDW-PLD state is driven by an anomaly in the generalized susceptibility resulting from the coupling of electronic states at the Fermi level (E_F) with phonon modes that have a displacement wave vector that spans heavily nested regions of the Fermi surface. Once in the CDW state, a gap opens up at E_F in the electron density of states [3]. While this model is quite satisfactory for quasi-1D conductors, its application to quasi-2D conductors is problematic, since the 2D susceptibility anomaly is much smaller. However, CDW-PLD instabilities have been observed in quasi-2D conductors, for example, in the purple molybdenum bronzes such as KMo_6O_{17} and $Na_{0.9}Mo_6O_{17}$ [4], in monophosphate tungsten bronzes [4] of the form $(PO_2)_4(WO_3)_{2m}$, and in organic conducting salts such as $(BEDT\text{-}TTF)_2ReO_4$ (where BEDT-TTF refers to bisethylenedithiotetrafulvalene). Whangbo *et al.* introduced the idea that the Fermi surfaces in these materials can be viewed as a combination of *quasi-1D* structures, with distinct 1D nesting vectors [1,2]. Indirect experimental confirmation of this model comes from x-ray diffraction measurements, which show that the displacement vector of the structural instability in KMo_6O_{17} and $Na_{0.9}Mo_6O_{17}$ are consistent with the predicted "hidden" quasi-1D nesting wave vector [1]. However, until now there have been no direct measurements of Fermi surfaces that exhibit such nesting.

We present here the first measurement of hidden Fermi surface nesting. The system studied was $Na_{0.9}Mo_6O_{17}$, which possesses a layered structure consisting of planes of Mo-O polyhedra separated by Na ions [5]. $Na_{0.9}Mo_6O_{17}$ exhibits quasi-2D transport properties within the (001) cleavage plane, and undergoes a metal-metal transition to a CDW state at 80 K [6]. (While Peierls transitions in 1D systems result in transitions to insulating CDW states, the CDW state in quasi-2D materials remains metallic, as the opening of a band gap occurs only over part of the Fermi surface.) The measurements reported here were made using angle resolved photoemission (ARP) spectroscopy [7–9]. The Fermi surface consists of hole and electron structures, and the observed nesting is in very good agreement with the calculated Fermi surface of Whangbo *et al.* [1]. Since hidden Fermi surface nesting is widely cited to explain CDW-PLD phenomena in organic and inorganic 2D conductors, this work has significant implications for our understanding of a wide class of materials [1,2].

Experiments were performed at the National Synchrotron Light Source (NSLS), on the Boston University–Bell Labs–NSLS bending magnet beam line U4A, which is equipped with a 6 m toroidal grating monochromator and a custom designed hemispherical electron analyzer [10]. Typical energy and full angular resolution were approximately 75 meV and 1°, respectively. All measurements were performed at room temperature, i.e., in the metallic state. Binding energies are referenced to E_F determined from an atomically clean Cu foil in electrical contact with the sample. Single crystals of $Na_{0.9}Mo_6O_{17}$ were grown by a temperature gradient flux technique [11], and all measurements were performed on crystals cleaved in the spectrometer chamber (base pressure $< 2 \times 10^{-10}$ Torr). Surfaces of quasi-low-dimensional transition metal oxides have been found to be sensitive to electron beam damage [12]. Consequently, low energy electron diffraction was not used to orientate *in situ* the crystals with respect to the spectrometer rotation axes and the incident photons. Instead, crystals were visually aligned in the spectrometer chamber, which is feasible due to their anisotropic shape, and the exact alignment of the axes determined by *ex situ* x-ray diffraction. The labeling of all spectra shown here has been corrected for the small offsets found. Fermi surface mapping with ARP

 0031-9007/96/76(17)/3172(4)$10.00

was performed in the conventional manner by defining a point on the Fermi surface by the location in k space where emission from a particular band disappears as the associated band disperses above E_F. This method is widely used and has been reviewed elsewhere [8,9].

Figure 1 shows two representative sets of ARP spectra taken with 18 eV photons. Only the energy region close to E_F is shown, and the spectral feature is due to emission from Mo 4d states. (The d character of these states was verified using resonant photoemission [13].) The onset of the O 2p emission occurs at 2.5 eV. The light was incident at 45° to the sample normal, approximately along the $\Gamma Y'$ direction in the rectangular surface Brillouin zone corresponding to the projected monoclinic unit cell. In this geometry, variation of the spectrometer angle θ corresponds to detecting electrons with momenta approximately along the $\Gamma Y'$ direction, while variation of the spectrometer angle ϕ corresponds to detecting electrons with momenta approximately along the $\Gamma X'$ direction. (The Brillouin zone and symmetry labels are shown in Fig. 2.) All angles are measured relative to the sample normal. Figure 1 presents data for two different values of ϕ, with θ varied in 2° steps, and corresponds to scanning through the Brillouin zone in two slices, parallel to $\Gamma Y'$. The full data set consists of many hundreds of spectra, with scans taken both parallel and perpendicular to $\Gamma Y'$.

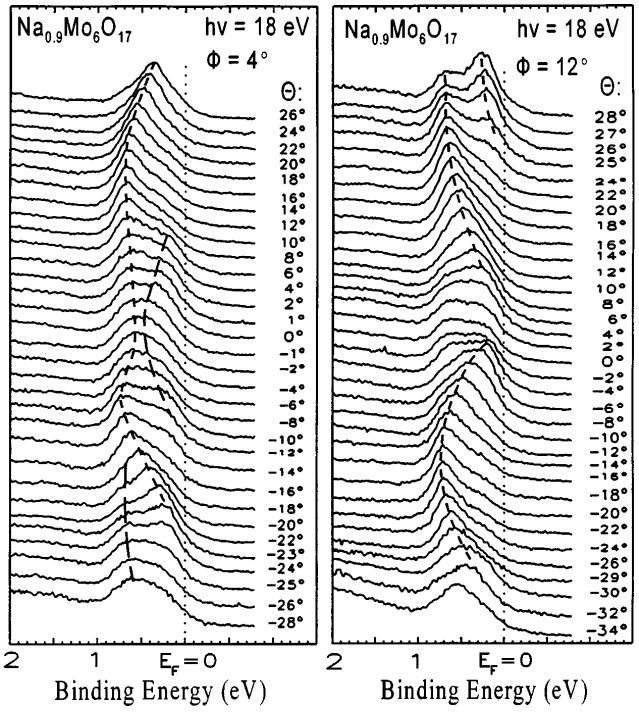

FIG. 1. ARP spectra from cleaved $Na_{0.9}Mo_6O_{17}$. $h\nu$ = 18 eV, incident at 45° to the sample normal in the $\Gamma Y'$ plane. Variation in θ and ϕ corresponds approximately to the $\Gamma Y'$ and $\Gamma X'$ directions in the Brillouin zone, respectively. See text for details. The surface Brillouin zone is shown in Fig. 2.

The spectra in Fig. 1 show remarkably clear band dispersion, particularly for a transition metal oxide, and equally clear dispersion was observed for all spectra from this material. There are three occupied Mo 4d bands in $Na_{0.9}Mo_6O_{17}$, which are predicted to form three distinct Fermi surface structures as they cross E_F [14]. Consequently, the spectral feature extending between 0 and 1 eV below E_F is comprised of emission from up to three d bands, depending on the location in the Brillouin zone. As a guide to the eye, the dispersion of the primary features of the spectra have been marked. Considering the $\phi = 12°$ set of spectra in Fig. 1, a symmetric dispersive feature is clearly visible on both sides of $\theta = 0°$. This is designated as band 1. As θ is varied from $-30°$ to $-20°$, band 1 disperses away from E_F to higher binding energies, reaching a maximum binding energy of 700 meV, then disperses back towards E_F as θ approaches zero, disappearing above E_F at approximately $-4°$. The peak reappears for $\theta > +4°$, and proceeds to disperse to higher binding energies. Clearly band 1 forms a hole pocket in the Fermi surface centered around the $\Gamma X'$ axis ($\theta = 0°$). (Note that the Γ point is $\theta = 0°$, $\phi = 0°$.) The spectra in the left-hand panel of Fig. 1 are equivalent to the spectra in the right-hand panel, but with $\phi = 4°$. Thus these spectra also show emission from states in a slice through the zone parallel to $\Gamma Y'$, but closer to Γ. Here, band 1 approaches, but does not cross E_F, indicating the closure of the hole pocket.

Further examination of the $\phi = 4°$ spectra in Fig. 1 reveals that a second feature near E_F is visible in the vicinity of Γ when band 1 has dispersed far below E_F. This emission is unrelated to band 1, and is designated as band 2. Unlike band 1, this feature disperses to *higher* binding energy near Γ, attaining a binding energy of 350 meV at Γ, where it essentially coincides with band 1.

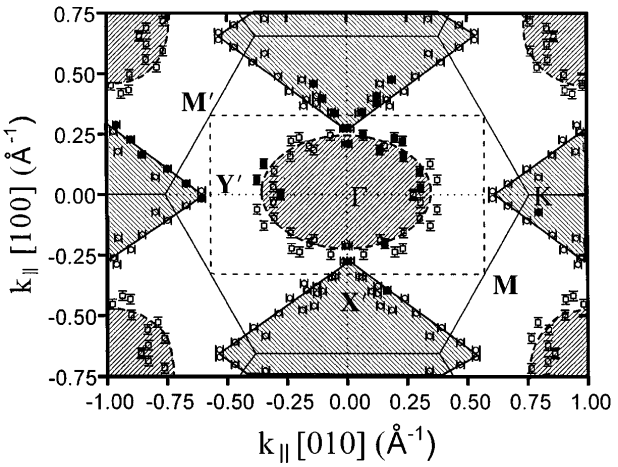

FIG. 2. Measured Fermi surface of $Na_{0.9}Mo_6O_{17}$. Band 1 data = ●, band 2 data = ■; hollow symbols indicate symmetry mapped points. The projected monoclinic and pseudo-hexagonal Brillouin zones are indicated. See text for details.

Band 2 disperses towards E_F on both sides of Γ, and disappears at approximately $-12°$ and 8°, respectively. Thus band 2 is found to form an electron pocket in the Fermi surface. The exact positions of the Fermi level crossings associated with band 2 can be determined with a much better accuracy for scans where k is varied along the $\Gamma X'$ direction (not shown).

Additional Fermi surface crossings are visible in both sets of spectra in Fig. 1. These correspond to Fermi surface structures in the second Brillouin zone. For example, there is a clear crossing visible in the $\phi = 12°$ spectra when the peak that dominates the spectrum at $\theta = 28°$ disperses towards E_F and crosses at approximately $\theta = 24°$. From symmetry arguments presented below, this is, in fact, band 2 crossing E_F in the second zone.

By scanning the entire surface Brillouin zone in a manner similar to that described above, the full Fermi surface was measured, and is presented in Fig. 2. Here crossings of E_F by band 1 are displayed as circles, while crossings of band 2 are shown as squares. Filled symbols correspond to the measured data points, hollow symbols indicate symmetry mapped points. The performed symmetry operations consist of reflections about the $\Gamma X'$ and $\Gamma Y'$ axes, and of translations by lattice vectors of the "pseudohexagonal" zone. This symmetry reflects the pseudohexagonal character of the bulk crystal structure. The choice of unit cell and the validity of these symmetry operations can be directly extrapolated from the experimental data. The spectra in Fig. 1 reveal that band 1 can be measured in the second zone, irrespective of the choice of the zone (monoclinic or hexagonal). The Fermi surface in Fig. 2 is shown with respect to the rectangular cell that follows from the projection of the bulk monoclinic unit cell onto the surface and also with respect to a hexagonal cell that has twice the volume. The hexagonal cell would be correct if the angle between the [100] and the [001] axis was not 89.94°, but 90°, as this leads to a trigonal cell equivalent to that of the structurally very similar material KMo_6O_{17} [4,15]. The choice of the surface unit cell is therefore not obvious. However, the measured Fermi surface consists of two distinct types of structures: a closed electron pocket (roughly elliptical in shape) around Γ formed by band 2, and hole pockets (roughly diamond shaped) along $\Gamma X'$ and $\Gamma Y'$, formed by band 1 (Fig. 2). (Note that the lines drawn in Fig. 2 are guides to the eye, and not fits to the data points; they emphasize the observation of two distinct types of structures.) It is evident that only translations with vectors of the hexagonal lattice produce a periodic Fermi surface. At the same time, the only valid symmetry operations are those compatible with the monoclinic symmetry. Consequently, this symmetry can be labeled as pseudohexagonal.

Inspection of Fig. 2 shows that the Fermi surfaces of the electron and hole pockets can be combined to form almost uninterrupted *pseudo-1D* Fermi surfaces parallel to the $\Gamma M'$ axes of the rectangular zone. These 1D Fermi surfaces are drawn in Fig. 3, where the same data points are shown as in Fig. 2. A pair of lines running parallel to $\Gamma M'$ connects both the electron and hole structures shown in Fig. 2. This is precisely the Fermi surface nesting postulated by Whangbo *et al.* [1]. Although the calculations were performed for KMo_6O_{17}, the authors argue that the results also apply to $Na_{0.9}Mo_6O_{17}$, as both oxides are structurally similar. Figures 4(a), 4(b), and 4(c) show the calculated Fermi surfaces for the three *d* bands that are predicted to cross the Fermi level. The combination of these three Fermi surfaces is shown in Fig. 4(d). When combined, these Fermi surfaces lead to three quasi-1D Fermi surfaces parallel to the ΓM direction as drawn in Fig. 4(e). The nesting of this hidden Fermi surface corresponds to the displacement vectors that are associated with the superlattice spots observed below the critical temperature for the Peierls transition. As can be seen in Fig. 4(f), two pairs of quasi-1D Fermi surface segments can be connected to each other by the same vector q, thereby maximizing the nesting. The calculations in Fig. 4(f) can be compared directly with the measured Fermi surface of Fig. 3. To within experimental error, the measured quasi-1D nesting vector ($2k_F = 0.67$ Å^{-1}) is essentially identical both to the predicted value and also to the displacement vector given by the KMo_6O_{17} x-ray diffraction data [1,16].

Despite our observation of nesting of the correct magnitude and direction to explain the observed lattice distortion, there are two significant differences between the calculated Fermi surface for KMo_6O_{17} and our measurement for $Na_{0.9}Mo_6O_{17}$. The first is that while the calculations predict two electron pockets centered around the Γ point, only one such structure is observed. A third band is observed in the spectra, but it does not cross E_F. This feature is most clearly visible in Fig. 1 at regions of the zone where bands 1 and 2 have crossed E_F. The second difference is that there is no evidence for a 1D Fermi surface

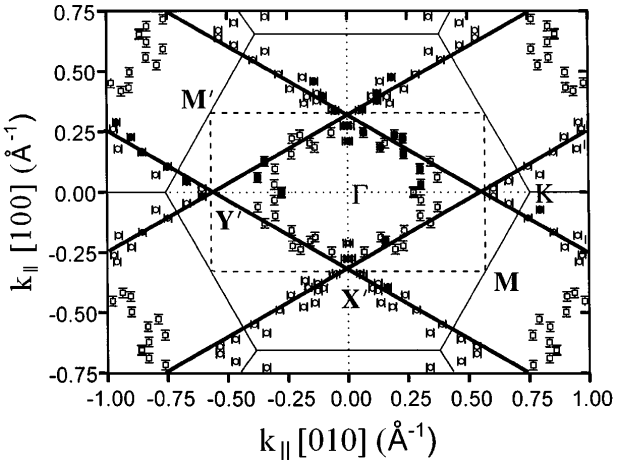

FIG. 3. Same data as in Fig. 2, but with the "hidden" quasi-1D Fermi surfaces indicated. See text for details.

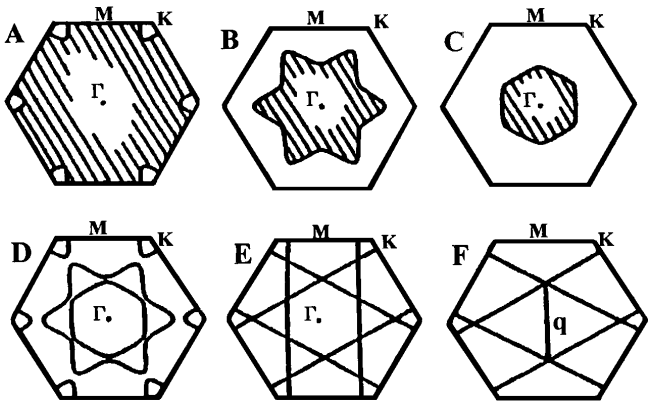

FIG. 4. Predicted Fermi surface for KMo_6O_{17} from tight binding calculations of Ref. [1]. (a)–(c) Individual Fermi surfaces from three distinct bands; (d) full Fermi surface; (e) "hidden" 1D Fermi surfaces; and (f) nesting wave vector q connecting two 1D Fermi surfaces.

structure parallel to the $\Gamma X'$ direction (Fig. 2). Along $\Gamma X'$ the bands behave quite differently than predicted from the calculation with the hexagonal symmetry. This direction, which corresponds to the projected [100] axis, is precisely the direction in which symmetry is broken when the trigonal cell of KMo_6O_{17} is modified to form a monoclinic cell in $Na_{0.9}Mo_6O_{17}$. While many features of the Fermi surface maintain their identity in the monoclinic symmetry, there appear to be symmetry induced changes of the Fermi surface resulting in modified nesting properties. This may explain why the electronic properties of purple bronzes are not identical, as it is the case for the blue bronze series ($A_{0.3}MoO_3, A$ = alkali). While the nesting vectors in $Na_{0.9}Mo_6O_{17}$ and KMo_6O_{17} are believed to be identical, the transition temperatures to the CDW state are different [16]. KMo_6O_{17} undergoes a transition at 120 K while $Na_{0.9}Mo_6O_{17}$ becomes unstable at 80 K. This indicates that there are significant changes in the electronic structure due to the quite subtle changes of the crystal structure [11].

In conclusion, the full Fermi surface of the quasi-2D conductor $Na_{0.9}Mo_6O_{17}$ has been measured and found to exhibit the predicted hidden quasi-1D Fermi surface nesting. The concept of hidden Fermi surface nesting is thus verified, supporting the identification of the metal-metal transitions in inorganic and organic quasi-2D conductors as Peierls transitions.

We thank G. Morales and K. F. Ludwig for the x-ray diffraction alignment measurements. We also are happy to acknowledge numerous useful discussions with M.-H. Whangbo. This work was supported in part by the National Science Foundation under CAREER Award No. DMR-9501174, and by the donors of the Petroleum Research Fund, administered by the American Chemical Society. Research was undertaken at the NSLS, which is supported by the U.S. DOE, Divisions of Materials and Chemical Sciences.

*Present address: Institut de Physique, Université de Neuchâtel, CH-2000 Neuchâtel, Switzerland.
†On leave from the Institute of Microtechnology, Bucharest, Romania.
‡To whom correspondence should be addressed.

[1] M.-H. Whangbo, E. Canadell, P. Foury, and J.-P. Pouget, Science **252**, 96 (1991).
[2] M.-H. Whangbo, J. Ren, W. Liang, E. Canadell, J.-P. Pouget, S. Ravy, J. M. Williams, and M. A. Beno, Inorg. Chem. **31**, 4169 (1992).
[3] For a general discussion, see *Crystal Chemistry and Properties of Materials with Quasi-One-Dimensional Structures*, edited by J. Rouxel (D. Reidel Publishing, Dordrecht, 1986).
[4] *Low Dimensional Electronic Properties of Molybdenum Bronzes and Oxides*, edited by C. Schlenker (Kluwer Academic Publishers, Dordrecht, 1989).
[5] M. Onoda, Y. Matsuda, and M. Sato, J. Solid State Chem. **69**, 67 (1987).
[6] M. Greenblatt, K. V. Ramanujachary, W. H. McCarroll, R. Neifeld, and J. V. Waszcak, J. Solid State Chem. **59**, 149 (1985).
[7] E. W. Plummer and W. Eberhardt, Adv. Chem. Phys. **49**, 533 (1982).
[8] K. E. Smith and S. D. Kevan, Prog. Solid State Chem. **21**, 49 (1991).
[9] For a review of ARP applied to quasi-low-dimensional conductors, see K. E. Smith, Ann. Rep. Prog. Chem. C **90**, 115 (1993).
[10] S. D. Kevan, Rev. Sci. Instrum. **54**, 1441 (1983).
[11] M. Greenblatt, Chem. Rev. **88**, 31 (1988).
[12] K. Breuer, K. E. Smith, M. Greenblatt, and W. McCarroll, J. Vac. Sci. Technol. A **12**, 2196 (1994).
[13] K. Breuer, C. Stagarescu, K. E. Smith, M. Greenblatt, and K. Ramanujachary (unpublished).
[14] M.-H. Whangbo, E. Canadell, and C. Schlenker, J. Am. Chem. Soc. **109**, 6308 (1987).
[15] H. Vincent, M. Ghedira, J. Marcus, J. Mercier, and C. Schenker, J. Solid State Chem. **47**, 113 (1983).
[16] C. Escribe-Filippini, K. Konate, J. Marcus, C. Schlenker, R. Almairac, R. Ayroles, and C. Rouacau, Philos. Mag. B **50**, 321 (1984).